








RESEARCH ARTICLE | DECEMBER 28 2021

Cryo spectroscopy of N_2 on cationic iron clusters

Annika Straßner ; Christopher Wiehn; Matthias P. Klein ; Daniela V. Fries ; Sebastian Dillinger; Jennifer Mohrbach; Marc H. Prosenč ; P. B. Armentrout ; Gereon Niedner-Schatteburg  



J. Chem. Phys. 155, 244305 (2021)

<https://doi.org/10.1063/5.0064966>



Boost Your Optics and
Photonics Measurements

Lock-in Amplifier

 Zurich
Instruments

[Find out more](#)

Boxcar Averager

Cryo spectroscopy of N₂ on cationic iron clusters

Cite as: J. Chem. Phys. 155, 244305 (2021); doi: 10.1063/5.0064966

Submitted: 28 July 2021 • Accepted: 25 October 2021 •

Published Online: 28 December 2021



View Online



Export Citation



CrossMark

Annika Straßner,¹ Christopher Wiehn,¹ Matthias P. Klein,¹ Daniela V. Fries,¹ Sebastian Dillinger,¹ Jennifer Mohrbach,¹ Marc H. Prosenč,¹ P. B. Armentrout,² and Gereon Niedner-Schatteburg^{1,a)}

AFFILIATIONS

¹ Fachbereich Chemie and Forschungszentrum OPTIMAS, Technische Universität Kaiserslautern, 67663 Kaiserslautern, Germany² Department of Chemistry, University of Utah, Salt Lake City, Utah 84112, USA^{a)} Author to whom correspondence should be addressed: gns@chemie.uni-kl.de.

TU Kaiserslautern, Fachbereich Chemie: Erwin-Schrödinger-Straße 52, 67663 Kaiserslautern, Germany

ABSTRACT

Infrared photodissociation (IR-PD) spectra of iron cluster dinitrogen adsorbate complexes $[\text{Fe}_n(\text{N}_2)_m]^+$ for $n = 8\text{--}20$ reveal slightly redshifted IR active bands in the region of $2200\text{--}2340\text{ cm}^{-1}$. These bands mostly relate to stretching vibrations of end-on coordinated N₂ chromophores, a $\mu_{1,\text{end}}$ end-on binding motif. Density Functional Theory (DFT) modeling and detailed analysis of $n = 13$ complexes are consistent with an icosahedral Fe₁₃⁺ core structure. The first adsorbate shell closure at $(n, m) = (13, 12)$ —as recognized by the accompanying paper on the kinetics of N₂ uptake by cationic iron clusters—comes with extensive IR-PD band broadening resulting from enhanced couplings among adjacent N₂ adsorbates. DFT modeling predicts spin quenching by N₂ adsorption as evidenced by the shift of the computed spin minima among possible spin states (spin valleys). The IR-PD spectrum of (17,1) surprisingly reveals an absence of any structure but efficient non-resonant fragmentation, which might indicate some weakly bound (roaming) N₂ adsorbate. The multiple and broad bands of (17, m) for all other cases than (17,1) and (17,7) indicate a high degree of variation in N₂ binding motifs and couplings. In contrast, the (17,7) spectrum of six sharp bands suggests pairwise equivalent N₂ adsorbates. The IR-PD spectra of (18, m) reveal additional features in the $2120\text{--}2200\text{ cm}^{-1}$ region, which we associate with a $\mu_{1,\text{side}}$ side-on motif. Some additional features in the (18, m) spectra at high N₂ loads indicate a $\mu_{1,\text{tilt}}$ tilted end-on adsorption motif.

© 2021 Author(s). All article content, except where otherwise noted, is licensed under a Creative Commons Attribution (CC BY) license (<http://creativecommons.org/licenses/by/4.0/>). <https://doi.org/10.1063/5.0064966>

I. INTRODUCTION

The interaction of small molecules such as NO, N₂, and H₂ with transition metals (TMs) is an early elementary step in heterogeneous catalysis.^{1–6} TM cations^{7–9} and TM clusters^{10–14} have served as model systems to mimic such catalysts and related elementary processes. TM cluster studies offer the opportunity to study TM-adsorbate interactions in analogy to TM surface studies.^{15,16} These include an early mass spectral (MS) investigation of N₂ chemisorption to Fe and Co clusters.¹⁷

N₂ activation is an early elementary process in the course of ammonia synthesis, catalyzed under extreme conditions by the Haber–Bosch process using Fe, Ni, Ru, and other TMs.^{16,18–21} It is often identified as the rate-determining bottleneck of the overall reaction. Early surface science studies investigated N₂ adsorption on various Fe surfaces.^{22–25} A subsequent study of N₂ adsorbates on the Fe(111) surface by Low-Energy Electron Diffraction (LEED) in

conjunction with early *ab initio* modeling identified α -N₂ and γ -N₂ binding motifs.²⁶ These observations may relate to variations in hapticities, namely, side-on (η^2) and end-on (η^1) coordination of N₂ to single metal centers, or variations in coordination, namely, on top of a single Fe center (μ_1), or bridging two centers (μ_2), or in the hollow of three centers (μ_3). A third β -N₂ motif was found by further spectroscopic investigations and describes a dissociative chemisorption of the N₂ molecule to the Fe(111) metal surface atoms.^{27,28} Further modeling identified various dissociation channels²⁹ and predicted the most favorable N₂ adsorption on a quadruple hollow site.³⁰ On a potassium promoted Fe(111) surface, Whitman *et al.* found ¹⁵N₂ vibrational frequencies of α -N₂ (1415 cm^{-1}) and γ -N₂ (2100 cm^{-1}) in vibrational and thermal-desorption spectra.³¹

The Infrared Multiple Photon Dissociation (IRMPD) method is established to elucidate vibrational modes of adsorbates on TM clusters and TM coordination complexes as isolated ions.^{32–35} Its spectral range was extended by the advent of Free Electron Lasers (FELs)

in the IR.^{36–38} The brute force IRMPD method may turn into a more gentle single photon IR-PD method when ensuring a low fragmentation threshold, e.g., by the cryo mediated attachment of weakly bound chaperones that do not disturb other important features. Such an approach is labeled a tagging or messenger technique.^{39–43} Of course, molecular tags may turn into chromophores, and that is the case when utilizing N₂.⁴⁴

The tagging approach has proven successful and gained further insight into the adsorbate cluster interaction, for instance, in the case of Fe clusters with H₂ or water. IR spectroscopic characterization of Fe_n⁺ cluster H₂ adsorbate complexes has revealed the formation of twofold or threefold coordinated hydrides, whereas related studies of extended metal surfaces revealed a preference for exclusively high hydride coordination, threefold or higher, and migration into the bulk.⁴⁵ Somewhat surprisingly, the water hydrolysis by cationic Fe clusters increases with cluster size.⁴⁶ FEL studies of Fe cluster CO adsorbate complexes revealed systematic cluster size and charge effects.^{47–49}

At this point, it becomes beneficial to realize that the carbon monoxide molecule, CO, is one of the most widely studied ligands, and its composite binding mechanism is claimed to be well understood. The composite CO–TM binding is described in terms of a concerted σ -donation from CO to TM and a π -backdonation from TM to CO, as described for the case of TM surfaces⁵⁰ and for the cases of single TM centers in coordination compounds.^{51,52} In both cases, the CO–TM interactions lead to noticeable redshifts of CO vibrations with a diagnostic value. In strong analogy, all of these concepts transfer to the characterization of CO–TM cluster interactions^{53–56} and to N₂–TM interactions, N₂ being isoelectronic with CO and polarizing upon TM interaction.

Fundamentals of how nitrogen interacts with TM cations (TM = V, Nb, and Rh) were clarified by application of IRMPD spectroscopy in the Duncan group.^{57–59} The Fielicke group studied N₂ on neutral Ru clusters and identified exclusively end-on (η^1) coordination.⁶⁰ Discrete Fourier transform (DFT) modeling of N₂ on a Ru surface predicted activation barriers and active sites at the level of pure DFT functionals.⁶¹

It is a mandatory complement to augment spectroscopy by quantum chemical modeling of investigated systems whenever possible. Numerous theoretical studies dealt with the modeling of small, bare Fe clusters, investigating their structure, energetics, and magnetic moments.^{62–70} N₂ interactions with Fe clusters received attention in the course of further DFT modeling studies, all of which concluded in a strong preference of N₂ end-on coordination to single Fe centers.^{71,72} Most recent DFT modeling deals with the coalescence of iron nitride clusters and concomitant spin reduction, leaving open the question whether pure DFT functionals are applicable.⁷³

Iron cluster cation chemistry has been explored using guided ion beam tandem mass spectrometry (GIBMS) at the University of Utah. After initial measurements of the cluster binding energies by collision-induced dissociation (CID) with Xe,^{74,75} thermochemistry for reactions of Fe_n⁺ with D₂ ($n = 2–15$),⁷⁶ O₂ ($n = 2–18$),⁷⁷ CO₂ ($n = 1–18$),⁷⁷ and CO ($n = 1–17$)⁴⁹ was examined. Of direct relevance to the present work, reactions of Fe_n⁺ ($n = 1–19$) with N₂ and ND₃ were examined and Fe_n⁺–N and Fe_n⁺–2N bond energies were measured.^{78,79} An activation barrier of 0.48 ± 0.03 eV was determined for activation of N₂ by the larger clusters ($n = 12, 15–19$).

With the tandem cryo ion trap instrument^{44,80} at the Technische Universität Kaiserslautern (TUK) laboratory, we are able to conduct Infrared Photon Dissociation (IR-PD) spectroscopy experiments at temperatures down to 11 K, as well as adsorption and reaction kinetics studies. With this combination of methods, we were able to study the cluster-adsorbate-interaction of various TM clusters, e.g., for Ni_n⁺ clusters, we established a concept of size-dependent rough and smooth cluster surfaces.^{80–82} We transferred this concept to the N₂ adsorption on Rh_n⁺⁸³ and Co_n⁺⁴⁴ clusters. With the ability to introduce different reaction gases into two subsequent cryo ion traps, we were able to check the influence of one adsorbate on another and vice versa, applying (N₂, H₂) to Ru₈⁺ clusters.⁸⁴ Our recent IR-PD study of the N₂ activation by small Ta⁺ clusters revealed a multiple step activation pathway with submerged barriers.⁸⁵

The present study elucidates the vibrational spectroscopy of N₂ adsorbates onto cationic iron clusters [Fe_n(N₂)_m]⁺ ($n = 8–20$). It obtains strong support of its findings through our adjoined cryogenic kinetic study,⁸⁶ which we will refer to as CKS in the following. We gain insights into coordination motifs and interactions of N₂ adsorbates, and we receive some decisive support from our concomitant DFT modeling at the level of hybrid DFT functionals. These methods are not easily applied in the cases of larger clusters.

II. EXPERIMENTAL AND COMPUTATIONAL METHODS

All experiments were performed in a customized Fourier Transform Ion Cyclotron Resonance (FT-ICR) mass spectrometer (Apex Ultra Bruker Daltonics). It was used to perform the cluster production, isolation, N₂ condensation, IR-PD spectroscopy, and mass analysis. For a detailed description of the formation of the cluster adsorbate complexes, refer to CKS. As for those kinetic studies, the clusters and their adsorbate complexes were stored for spectroscopic interrogation within the RF hexapole ion trap in conjunction with a He buffer gas at 26 K. This ensures equilibrated cluster ion temperatures of below 40 K under any circumstances.

The IR-PD spectra were measured by coupling the FT-ICR cell to a tunable IR laser (spectral resolution: $\delta n = 0.9$ cm⁻¹ and pulse length $\delta t = 10$ ns). This laser is a KTP/KTA optical parametric oscillator/amplifier (OPO/A, LaserVision) system pumped by a pulsed 10 Hz injection seeded Nd:YAG laser (PL8000, Continuum). The following AgGaSe₂ crystal generates the difference frequency (DF) between the optical parametric amplifier (OPA) signal and idler waves and generates IR radiation in the range of 1000–2400 cm⁻¹. Each trapped and isolated ion packet is irradiated by 7–10 laser pulses (0.1–3.5 mJ/pulse) to create a sufficient amount of fragment ions. The IR-PD spectra were recorded as ion chromatograms while continuously scanning the IR wavelength. The IR-PD signal was evaluated as fragmentation efficiency = $\frac{\sum_i F_i}{\sum_i F_i + \sum_i P_i}$, where F_i and P_i indicate the fragment and the parent ion signals. An experimental IR-PD spectrum results from a plot of the fragmentation efficiency as a function of the laser frequency. The IR-PD spectra were recorded in the range of 1980–2340 cm⁻¹ on the [Fe_n(N₂)_m]⁺ = (n, m) species ($n = 8–20$). One or two photons provide sufficient energies to induce loss of a single N₂ adsorbate, which is predicted by our DFT modeling (see below) to be bound by about 30–50 kJ/mol (see, e.g., Fig. 11). For all complexes, the loss of single or multiple N₂ was the only observed fragmentation channels.

All density functional theory calculations, including geometry optimizations, and vibrational analysis, were performed using the Gaussian 09⁸⁷ and Gaussian 16⁸⁸ packages with the pure and hybrid exchange–correlation functionals Perdew–Burke–Ernzerhof (PBE),⁸⁹ PBE0,⁹⁰ and TPSSh^{91,92} for small clusters and the pure DFT functional PBE for the large ones. We utilized the Ahlrichs/Weigend effective core potential (ECP) basis set def2TZVP throughout.⁹³ We checked all obtained minimum structures for lack of imaginary frequencies. The computed IR spectra at the PBE0/def2TZVP level were scaled by a factor of 0.971 to account for prevailing anharmonicities, and they were convoluted by application of a Lorentz profile with FWHM = 5 cm⁻¹. All other obtained spectra are documented in the SI without scaling. We envisage our current DFT results as “exploratory,” and we rate them as a starting point for further and more elaborate calculations.

III. RESULTS AND DISCUSSION

A. First and second N₂ adsorption

In order to augment our kinetic findings (CKS), we recorded IR-PD spectra of the cluster adsorbate complexes [Fe_n(N₂)₁]⁺, abbreviated (*n*,1), and [Fe_n(N₂)₂]⁺, abbreviated (*n*,2), for *n* = 8–20. We recorded all of their spectra in the region of 1980–2340 cm⁻¹ (Fig. S1), and we recorded some further spectra of (18,16) and (13,6) in the region of 1150–2400 cm⁻¹ (Figs. S2 and S3). In summary, none of these spectra exhibited IR-PD bands below 2150 cm⁻¹. In the following, we focus on an analysis of the region from 2150 to 2340 cm⁻¹ (Fig. 1).

All species, except [Fe₁₇(N₂)₁]⁺, show at least one IR active band in the investigated region, and this band is most likely associated with stretching vibrations of end-on coordinated N₂ chromophores. The (*n*,1) and (*n*,2) species with *n* = 11, 12, 16, and 18 exhibit a slightly shifted second band each, and the (*n*,2) species with *n* = 8, 17, 19, and 20 reveal such a second band, while the corresponding (*n*,1) species do not. The appearance of a second band may originate from Fe_n⁺ cluster core isomers, from the presence of non-equivalent adsorption sites, or from different spin states of the cluster.

In general, these N₂ adsorbate bands are significantly redshifted with respect to the free N₂ stretching frequency (2330 cm⁻¹).⁹⁴ This redshift is a result of the σ -donor π -acceptor synergism that weakens the N–N bond. The Blyholder model⁵⁰ has established this concept for CO adsorbates on metal surfaces, and in our earlier studies, we have adapted it for N₂ adsorbates on Co, Ni, Ru, or Rh.^{44,80,81,83,84} As compared to the N₂ adsorption on cationic Co and Ni clusters,^{44,80,81} the present N₂ adsorbate bands are less redshifted with respect to the free N₂ stretching frequency.

Looking at the spectra in more detail, one can perceive several special features. The most conspicuous feature is the missing band in the (17,1) spectrum and—in contrast—the appearance of two bands in the (17,2) spectrum. Also noticeable is the shift of the narrow N₂ band of (13,1) to that of (13,2) by 12 cm⁻¹. The spectra of the (18,1) and (18,2) species are the only ones that exhibit additional but weak IR-PD signal below 2250 cm⁻¹. These broad bands are located around 2200 cm⁻¹, which is 90 cm⁻¹ to the red of the strong N₂ stretching band in (18,1) and (18,2). Note that the Fe₁₈⁺ cluster shows special behavior in the kinetic studies in the form of a less-reactive isomer (CKS). The 2200 cm⁻¹ bands in the IR-PD

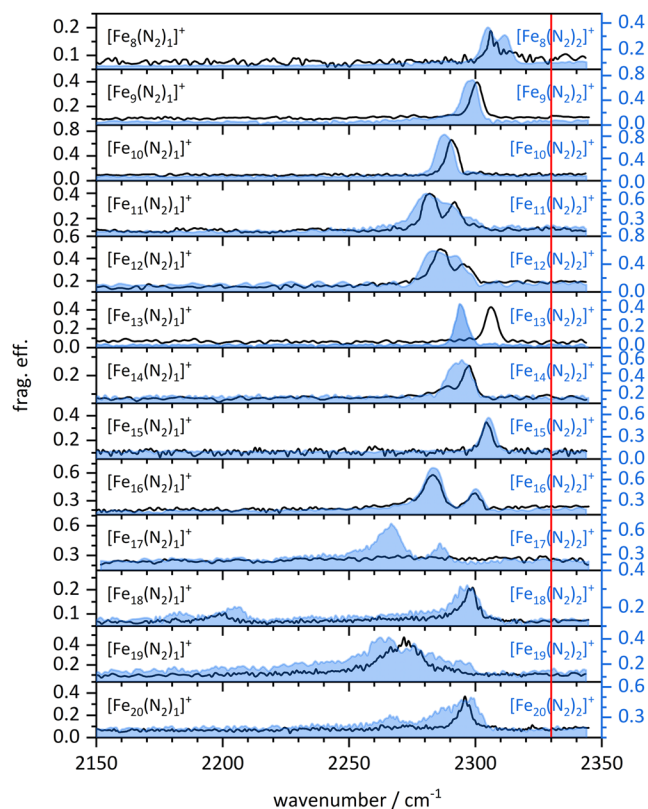


FIG. 1. IR-PD spectra of (*n*,1) (solid lines) and (*n*,2) (blue shades areas) species for *n* = 8–20 at 26 K. All bands are significantly red-shifted with respect to the free N₂ stretch (red line). In most cases, there are only subtle differences between the spectra of first and second N₂ adsorbates. Only for [Fe₁₃(N₂)_{1,2}]⁺ and [Fe₁₇(N₂)_{1,2}]⁺ are there considerable differences upon adsorption of the second N₂ molecule. The [Fe₁₆(N₂)_{1,2}]⁺ cluster adsorbate complexes are the only species that come with some weak bands around 2200 cm⁻¹.

spectra of (18,1) and (18,2) might be an indicator for an enhanced or a further auxiliary interaction between cluster and nitrogen adsorbate, which might point toward a precursor of nitrogen activation.

The (19,1) spectrum reveals a significantly broadened band (FWHM > 20 cm⁻¹) around 2270 cm⁻¹. For *n* = 11 and 12, the second separated band for the (*n*,1) species transforms more to a shoulder in the spectra for the (*n*,2). The cluster with *n* = 14 reveals a shoulder in the case of (14,1), which has merged with the primary band in the (14,2) spectrum.

Thus, the recorded IR-PD spectra indicate preferential end-on coordination of N₂ adsorbates and some extraordinary enhanced interaction in the case of *n* = 18. Other more involved and activating types of N₂ binding, as known from surface studies, would lead to spectral features far below 2000 cm⁻¹.^{27,95} Our own calculations confirm that bridging motifs have IR absorptions in a much lower wavenumber range than investigated here (Fig. S14).

In summary, the observed peak positions of first and second N₂ adsorbates, likely end-on, reveal little to no systematic variation

(cf. Figs. 1 and 2), but for some solitary exceptions, that might result from specific adsorption sites and/or symmetric/antisymmetric couplings of adjacent N_2 chromophores. We take this finding as an indication for a largely equivalent bonding situation of the first and second N_2 on the Fe_n^+ cluster surface. The only exception is the Fe_{18}^+ cluster, which reveals some indication for an N_2 preactivating binding motif.

There are no clear trends of N_2 vibrational frequencies with cluster size, as observed in cationic Ni clusters and interpreted in terms of a charge dilution model (Fig. 2, dashed line).⁸⁰ One might conceive a weak trend among small iron clusters ($n = 8-11$) but not for bigger ones ($n \geq 12$). Overall, by comparing the present data with those of N_2 adsorption on cationic Ni clusters, it is noticeable that the Fe clusters show remarkably different behavior.

B. Fe_{13}^+

The spectra of $(13, m)$, $m = 1-6$ and 12, reveal several special features (Fig. 3). The intensities of cluster adsorbate complexes with $m = 7-11$ are very low (cf. Fe_{13}^+ kinetics in CKS), and thus, it is not possible to record their IR-PD spectra. The Fe_{13} cluster provides special features in x-ray magnetic circular dichroism (XMCD) investigations and computational studies.⁹⁶⁻⁹⁸ These studies show a significant dip of the magnetic moment per atom as compared to other sized clusters. Our own exploratory DFT calculations of the Fe_{13}^+ geometry and spin states were performed at three different levels of theory: PBE, PBE0, and TPSSh using the def2TZVP basis set throughout. The hybrid DFT functionals PBE0 and TPSSh predict high multiplicities, $2S + 1 = 46$ of the bare Fe_{13}^+ cluster with icosahedral structure (Figs. S8-10), whereas the pure DFT functional PBE, void of exact exchange, predicts a lower multiplicity, $2S + 1 = 36$

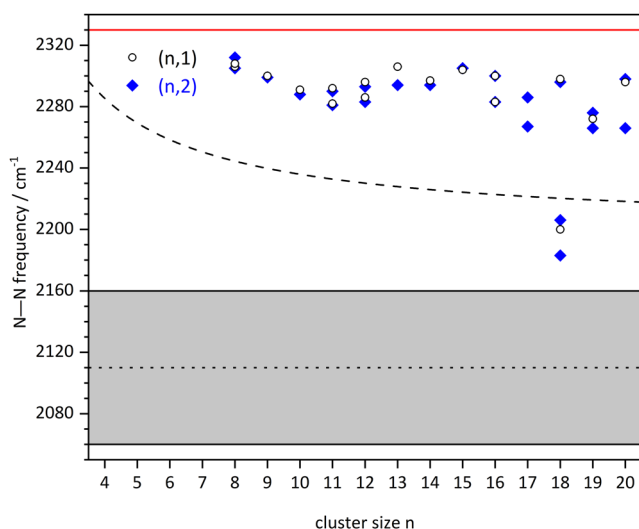


FIG. 2. N–N stretching frequency in $[Fe_n(N_2)_1]^+$ (black circles) and $[Fe_n(N_2)_2]^+$ (blue diamonds) for $n = 8-20$. The dashed line represents the trend of the N–N stretching frequency observed in cationic nickel clusters.⁸⁰ The red line is the stretching frequency of free N_2 . Also shown is the stretching frequency (black dotted line) with its FWHM (gray shaded area) of the so-called γ - N_2 on a clean iron surface, which is presumed to manifest some “on hollow” coordination, as revealed via vibrational EELS.⁹⁵

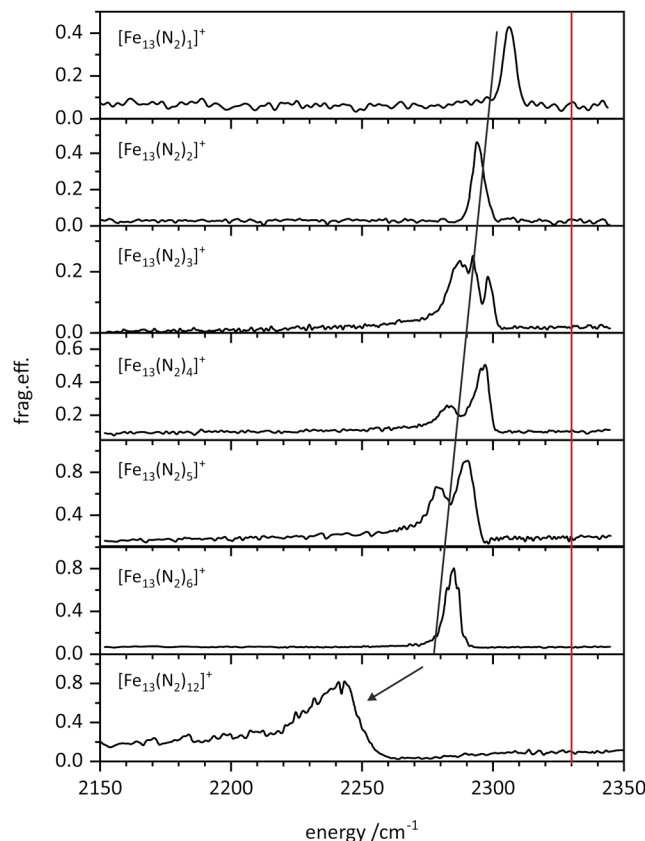


FIG. 3. IR-PD spectra of stepwise N_2 adsorption to the $(13, m)$ species at 26 K. From the narrow spectrum of the $[Fe_{13}(N_2)_6]^+$ cluster adsorbate complex, we deduce a highly symmetric geometry. There is a remarkable increase in the observed redshift from $(13, 6)$ to $(13, 12)$. The red vertical line indicates the stretching frequency of the free N_2 moiety.

(Figs. S8/S9). In the following, we primarily resort to results of the PBE0/def2TZVP level, which achieve the best agreement with the measured spectra using a scaling factor of 0.971. Results with the PBE functional (significantly smaller multiplicities and a scaling factor of significantly > 1) and with the TPSSh functional (at some points, different preferred structures and a scaling factor of ≈ 1) are included in the [supplementary material](#).

All of the measured IR active bands are redshifted with respect to the free N_2 stretching frequency (Fig. 3, red line). In a previous $Ta_4(N_2)_m$ study,⁸⁵ we identified a μ_2 - $\kappa N1:\kappa N1, N2$ across edge coordination motif and a μ_3 - $\kappa N1:\kappa N1, N2:\kappa N1, N2$ above surface motif, adopting the notation scheme of IUPAC and Salzer.⁹⁹ The latter does not apply in the current case of cryo N_2 spectra on Fe clusters; it would reveal much higher redshifts than observed. In any case, we utilize here the same nomenclature as in the tantalum case.

The (13,1) complex. We find a single sharp band at 2306 cm^{-1} (FWHM: 6 cm^{-1}). It seems reasonable at first sight that a highly symmetric icosahedron provides 12 equivalent adsorption sites, which leads to a single cluster adsorbate motif in the case of $(13, 1)$. This slightly redshifted band with respect to the free N_2 stretch

at 2330 cm^{-1} indicates the presence of a μ_1 end-on adsorbed N_2 molecule, as confirmed by our own exploratory DFT calculations (Fig. S14). Some of the structures obtained—(13,1)A through (13,1)E—are archetypical (Fig. 4), and they deserve special attention, also in light of the upcoming discussion of larger clusters, $m = 17, 18$. There are small variations in stretching frequency if end-on coordinated N_2 is slightly tilted as in (13,1)A across an edge ($\mu_1\text{-}\kappa\text{N1}(\text{:}\kappa\text{N1})$, 46tet, $^{102} 2304\text{ cm}^{-1}$) or as in (13,1)B above a triangular facet ($\mu_1\text{-}\kappa\text{N1}(\text{:}\kappa\text{N1}:\kappa\text{N1})$, 46tet, 2316 cm^{-1}) of the icosahedron. Spin quenching, from 46tet to 44tet as in (13,1)C, comes with a tilt above facet ($\mu_1\text{-}\kappa\text{N1}(\text{:}\kappa\text{N1}:\kappa\text{N1})$, 44tet, 2285 cm^{-1}). We classify all of these three related motifs as N_2 end-on coordination, $\mu_{1,\text{end}}$. The energetic expense of the tilting is merely 2 kJ/mol ; spin quenching adds an additional 15 kJ/mol .

There is another conceivable binding motif, (13,1)D, that comprises μ_2 bridging N_2 ($\mu_2\text{-}\kappa\text{N1}:\kappa\text{N1}, \text{N}_2$, 44tet, 1883 cm^{-1}). This motif provides a significantly more redshifted IR fingerprint than that observed [cf. Fig. S2 (18,16) and Fig. S3 (13,6) for a survey of the low-frequency ranges] and an energetic expense of $+29\text{ kJ/mol}$ with respect to the most favorable $\mu_{1,\text{end}}$ motif.

At an even higher energy of $+43\text{ kJ/mol}$, we find the (13,1)E structure, which provides an asymmetrically bound side-on N_2 ligand ($\mu_1\text{-}\kappa\text{N1}, \text{N}_2$, 44tet, 2152 cm^{-1}) that reveals a medium amount of vibrational redshift. This $\mu_{1,\text{side}}$ motif finds no experimental support in the case of a smooth icosahedral surface, (13,1), but it shall become a focus of interest in the course of the $m = 18$ discussion.

The (13,2) complex. The observed single band of (13,2) jumps by 12 to 2294 cm^{-1} , with respect to the corresponding band in (13,1). The lack of any second band points toward the equivalence of both N_2 adsorbates, in accord with an icosahedral core structure.⁹⁷ For our DFT exploration, we chose three positions of the second N_2 adsorbate with respect to the first one: A directly adjacent arrangement (pseudo-ortho), an arrangement of both N_2 adsorbates with one Fe site in between (pseudo-meta), and an arrangement with opposite N_2 adsorbates, which corresponds to a distance of two vacant Fe sites (pseudo-para) (Fig. S17). The most stable structure with at most a single stretching frequency at 2298 cm^{-1} is the 44tet with opposite N_2 adsorbates (Figs. S20/S21). This highly symmetric arrangement provides symmetrically and antisymmetrically coupled stretching vibrations of the two N_2 s. The symmetrically coupled

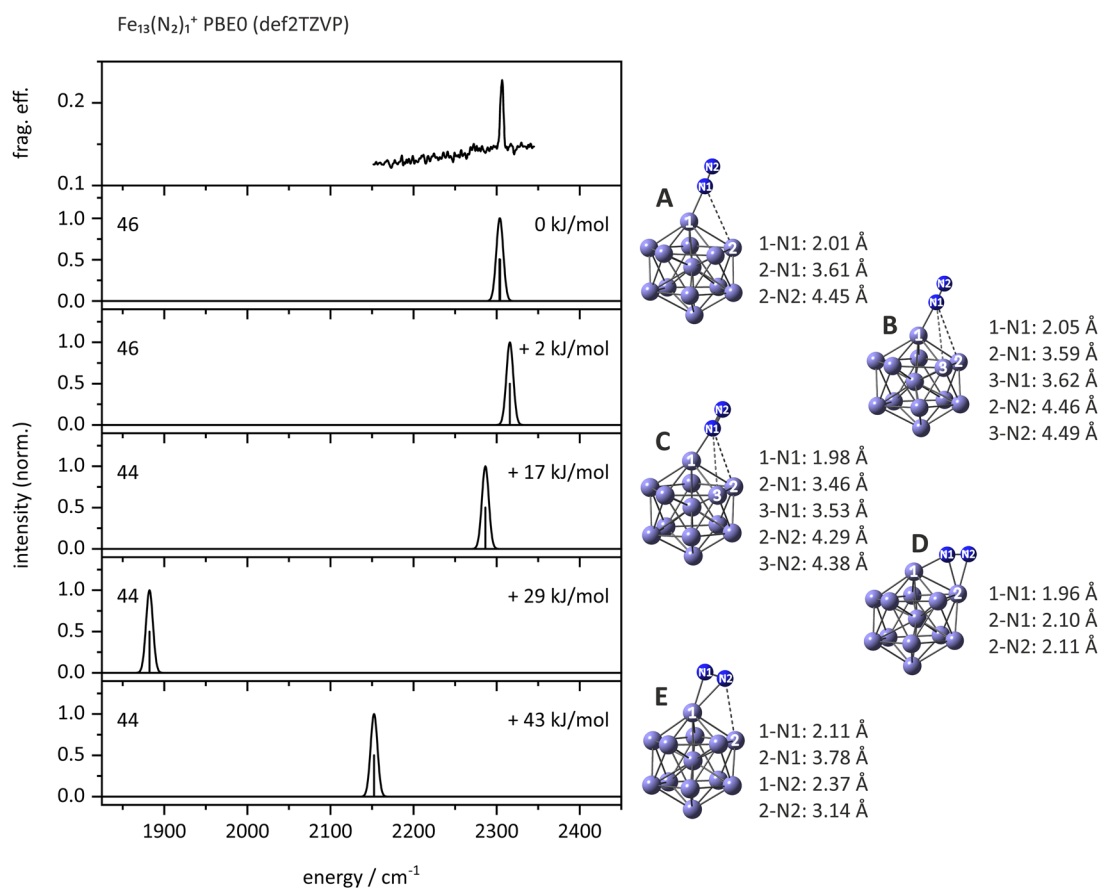


FIG. 4. Experimental IR-PD spectrum of (13,1) and DFT modeled spectra (PBE0/def2TZVP, scaling factor 0.971) with optimized cluster adsorbate structures and their Fe–N-bond lengths. End-on N_2 coordinations (A and B) match experiment the best. The asymmetric side-on coordination (E) is a motif that might become relevant at larger clusters (see the text).

stretching mode has very low IR intensity since no dipole moment changes by the vibration. The remaining antisymmetric stretching mode provides a single band. The calculated stretching frequency is 12 cm^{-1} shifted with respect to that of $[\text{Fe}_{13}(\text{N}_2)_1]^+ \text{A}$, in accord with the measured shift.

The (13,3) complex. In the spectrum of the (13,3) cluster adsorbate complex, we see three overlapping bands at 2287, 2292, and 2298 cm^{-1} . They indicate different adsorption sites, and they do not correspond exactly to any of the observed bands in (13,1) and (13,2). One might conceive a general shift by the amount of N_2 adsorption, as indicated by the diagonal line in Fig. 3. If so, then the 2294 cm^{-1} band in (3,2) corresponds to the 2287 cm^{-1} band in (13,3), and the 2306 cm^{-1} band in (13,1) corresponds to the 2298 cm^{-1} band in (13,3), making the 2292 cm^{-1} band in (13,3) a new feature. Of course, one has to keep in mind the known feature of symmetric and antisymmetric couplings of stretching modes in adjacent N_2 adsorbates.

By virtue of our DFT modeling, we identified five conceivable cluster adsorbate complexes of (13,3), with 3 N_2 molecules attached to the icosahedral surface (Fig. S25). A single structure includes the (13,2) adsorption motif [labeled (e) in Fig. S25], and this one turns out most favorable (by 15–21 kJ/mol) as compared to the other four structures (Fig. S28/S29). Third N_2 is added in the pseudo-ortho position to N_2 from the (13,2) motif, Fig. 5. Structure (e) assumes a 44tet, and it reveals three stretching frequencies at 2286, 2289, and 2303 cm^{-1} . The computed vibration at 2286 cm^{-1} originates from the antisymmetric stretching of the two adjacent N_2 molecules as in the (13,2) motif, and the symmetric combination appears at 2289 cm^{-1} . Both correspond well to the experimental bands at 2287 and 2292 cm^{-1} . The predicted vibration at 2303 cm^{-1} originates from the vibration of the sole distant N_2 molecule (Fig. 5), and it might correlate to the experimental band at 2298 cm^{-1} .

The (13,4) and (13,5) complexes. The IR-PD spectra of (13,4) and (13,5) reveal two bands each, which follow the general trend of shifts with the amount of N_2 adsorbates. Our exploratory quantum chemical modeling came close to interpret these bands but failed to obtain a close fit. We speculate that these bands might belong to vibrational motifs similar to (13,3), with the symmetric combination band being weak or blended.

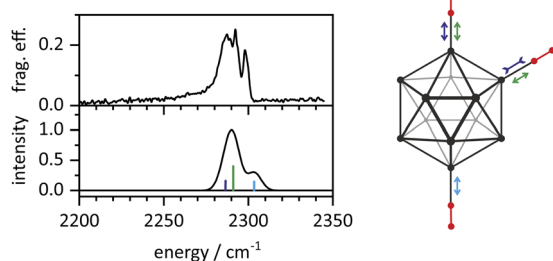


FIG. 5. Experimental IR-PD spectrum and DFT modeling of (13,3) vibrations. The computed structure is an icosahedron with a spin state of $2S + 1 = 44$. Three Fe centers adsorb an N_2 molecule each. The color-coding of the stick spectrum and the vibrational double arrow relate these to each other: the dark blue (antisymmetric) and green (symmetric), and the light blue represents stretching vibrations. The calculated spectrum is scaled for anharmonicity by 0.971. The central Fe atom and its coordination are omitted for clarity.

The (13,6) complex. The IR-PD spectrum of the (13,6) cluster adsorbate complex reveals a single, sharp band at 2285 cm^{-1} , with the same FWHM = 6 cm^{-1} as (13,1). We take both findings as strong evidence for high symmetry.

The anticipated icosahedral structure of naked Fe_{13}^+ provides a smooth cluster surface of 12 equivalent surface atoms. Seemingly, these 12 atoms might allow six equivalent adsorption sites. Our exploratory DFT modeling suggests the initial $\mu_{1,\text{end}}$ coordination of single N_2 adsorbates slightly tilted over an edge or face. Upon subsequent, multiple N_2 adsorptions of these slightly tilted end-on adsorbates result in a highly symmetric structure. Six of these motifs would fit on a single Fe_{13}^+ icosahedron. We find some evidence for such structures by our DFT modeling (Fig. 6), and the modeled vibrations come close to the experimental IR-PD spectrum (Fig. 7). Most noticeably, the single sharp band observed suggests that the vibrational couplings are weak, if present at all. This seems odd, given that all six N_2 adsorbates are adjacent to each other. In (13,2) and (13,3), such proximity leads to evident couplings and corresponding splittings. Their absence, or at least weakness, in (13,6) might indicate a considerable degree of N_2 tilting. As this coordinated, alternating tilting comes without vibrational coupling, the effect seems to relate to electronic coupling.

The (13,7) complex and beyond. As adsorption kinetics of the seventh N_2 is slow but speeds up considerably beyond, we failed to record IR-PD spectra of (13,7) through (13,11) because the ion intensities were extremely low. It looks as if the adsorption of seventh N_2 would be sterically hindered. Given a structure for (13,6) like that in Fig. 6, it seems conceivable that some reorganization of adsorbates needs to take place—in line with the observation of the low $k_{(13,6)}$ value (cf. CKS). After adsorption of seventh N_2 , a swift

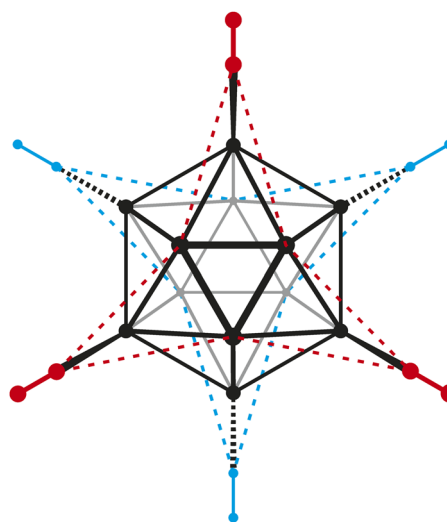


FIG. 6. A computed arrangement of six N_2 adsorbates with high symmetry in a $\text{Fe}_{13}(\text{N}_2)_6^+$ cluster adsorbate complex. The alternating tilting of N_2 ligands points out of plane to the front (red) and to the back (blue). The tilting of each end-on coordinated N_2 ligand occurs above a triangular facet toward a μ_3 -type coordination. We find N–N–Fe angles of 175° and N–Fe–Fe_{central} angles of 150° , with minor variations for all six N_2 adsorbates. The central Fe atom and its coordination are omitted for clarity, and we apply Natta projection to Fe–N bonds only.

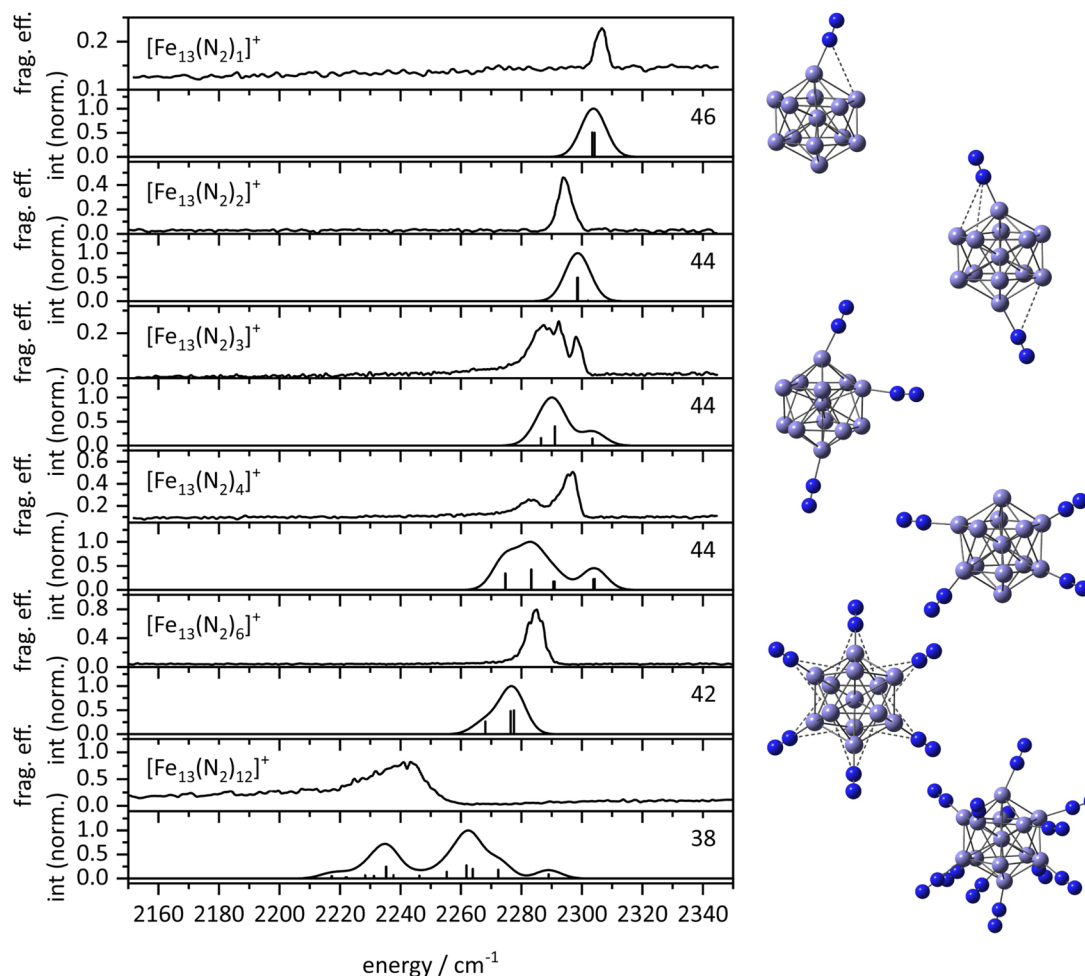


FIG. 7. Experimental IR-PD spectra and DFT modeled IR spectra of $(13,m)$, $m = 1-4, 6, 12$, at the PBE0/def2TZVP level (scaling factor: 0.971) and with most favorable multiplicity (as indicated); optimized structures are shown to the right of the DFT spectra. The modeling comes close to the observations, with differences in splittings and magnitudes. DFT modeling reaches its limits beyond $(13,12)$.

avalanche of further reorganization seems to occur such that adsorption to form $(13,12)$ is rapid. In **CKS**, we speculate about an adsorbate driven electronic reorganization of spin flips, which might act as the driving force. Further DFT modeling effort would be needed to come to more definite conclusions.

The $(13,12)$ complex. The IR-PD spectrum for the adsorption maximum, $m_{\max} = 12$, reveals a single broad, asymmetric band (FWHM = 18 cm^{-1}) with a long tail to the red. We speculate about two counteracting effects. A 1:1 stoichiometric, Langmuir-type end-on N_2 adsorption to each of 12 equivalent iron atoms on the icosahedron surface leads to a highly symmetric structure, and one might expect an IR-PD spectrum similar to that observed for $(13,6)$. On the other hand, the unavoidable proximity of the many N_2 molecules necessarily enables many mutual couplings that could lead to a significant broadening of otherwise equivalent IR stretching bands. In combination, a single shifted broad band might result. The observed magnitude of a $30\text{--}36 \text{ cm}^{-1}$ redshift going from $[\text{Fe}_{13}(\text{N}_2)_6]^+$ to

$[\text{Fe}_{13}(\text{N}_2)_{12}]^+$ is well in line with an observed redshift of $5\text{--}6 \text{ cm}^{-1}$ per additional N_2 ligand at smaller n . Our exploratory DFT calculations revealed multiple IR active N_2 stretching bands with many couplings that lead to a spreading out of bands across 100 cm^{-1} (Fig. 7).

The $(13, m)$ spin valleys by DFT. Although the IR-PD spectra do not provide information on the spin states of the cluster adsorbate complexes, the DFT calculations do. The results gain credibility through the favorable, yet qualitative modeling of the observed stretching vibrations. To verify this, however, we checked the relative stabilities of conceivable spin states of the studied cluster adsorbate complexes. Icosahedral Fe_{13}^+ geometries served as starting points, and we checked for full geometric relaxation of all nuclear degrees of freedom while maintaining full electronic convergence within the chosen quantum chemical model, the hybrid DFT functional PBE0, which comprises some admixture of Hartree-Fock-exchange and thus comes close to a valid

description of the actual electronics—excluding higher order effects such as spin–orbit coupling.

The total energies obtained are shown in Fig. 8 and correspond to the most stable adsorption isomers in all cases and form the basis for the following arguments. The results reveal an obvious so-called spin valley (as introduced before¹⁰⁰) with the highest stability of the naked Fe_{13}^+ at the spin multiplicity of $2S + 1 = 46$, a sextoquadragintet state. Notably, the adsorption of a single N_2 does not change this high-spin electronic arrangement, whereas the adsorption of two or more N_2 molecules does. In effect, there is a gradual spin quenching with progressive N_2 adsorption such that the (13,12) complex stabilizes at $2S + 1 = 38$. 12 N_2 adsorption events thus induce four instances of spin pairings. We have observed a similar spin-quenching phenomenon upon N_2 adsorption to Rh_5^+ clusters.¹⁰⁰

Although it is a challenge to interpret the observed spin quenching, it seems possible to speculate on the likely reasons. The naked Fe_{13}^+ cluster is superparamagnetic,^{96,98} and it is known to favor about three unpaired spins per atom on all of its surface atoms. These form a surface layer of singly occupied molecular orbitals (SOMOs) that exert Pauli repulsion to any closed-shell singlet state molecule (and N_2 is archetypical in this regard) that approaches. Thus, the molecule does not receive unpaired spin density. Donation of spin-paired electron density from the approaching N_2 to the cluster is thus hampered by the lack of accessible lowest unoccupied molecular orbitals (LUMOs), and the adsorption enthalpy will be small. This situation can change by turning pairs of cluster SOMOs into HOMO/LUMO pairs. The kinetic behavior provides some evidence that the concomitant promotion energy needed

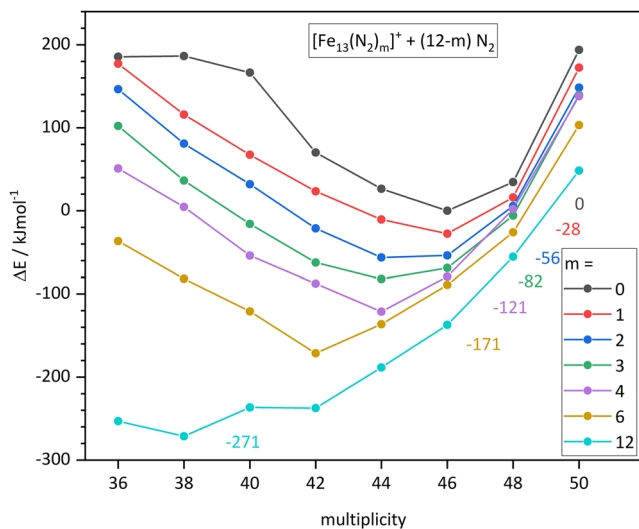


FIG. 8. Energetics of computed $[\text{Fe}_{13}(\text{N}_2)_m]^+$ cluster adsorbate complex structures as a function of the spin multiplicity $2S + 1$, normalized to the computed (13,0) spin isomer (icosahedron, 46tet) + 12 N_2 . The level of theory is PBE0/def2TZVP. Each depicted data point represents the optimized isomer of $[\text{Fe}_{13}(\text{N}_2)_m]^+$ in the given spin state. Connecting data of given m values yields the so-called spin valleys. The vertical offsets of adjacent curves indicate stepwise N_2 adsorption energies. Further spin-valley data at other levels of theory have similar shapes and are documented in the [supplementary material](#) (Figs. S4/S6).

for this conversion is overcompensated by the gain in adsorption enthalpy afforded by having an accessible LUMO for N_2 to bind. Thus, the rapid conversion of (13,6) to (13,12) is plausibly driven by this type of spin conversion. Accordingly, the spin valleys might be expected to shift stepwise toward lower multiplicities upon N_2 adsorption.

C. Fe_{17}^+

In the spectra of (17, m), where $m = 1-7$ and 9, we observe broad bands in all cases of cluster adsorbate complexes, except for (17,1), where no IR active band occurs, and (17,7), which exhibits six narrow separate bands. All of the observed bands are redshifted with respect to the free N_2 stretching frequency (Fig. 9, red line). Note that the generally noisy spectra suffer from the weak ion intensities of all investigated $[\text{Fe}_{17}(\text{N}_2)_m]^+$ cluster adsorbate complexes. This is partially because of the very slow N_2 adsorption for Fe_{17}^+ (cf. Fe_{17}^+ kinetics in CKS). In addition, there is a high level of non-resonant fragmentation of about 20%–30% under present conditions, which is significantly less for all other cluster sizes n .

It is somewhat surprising to recognize the absence of any structure in the spectrum of (17,1) but with reasonably efficient

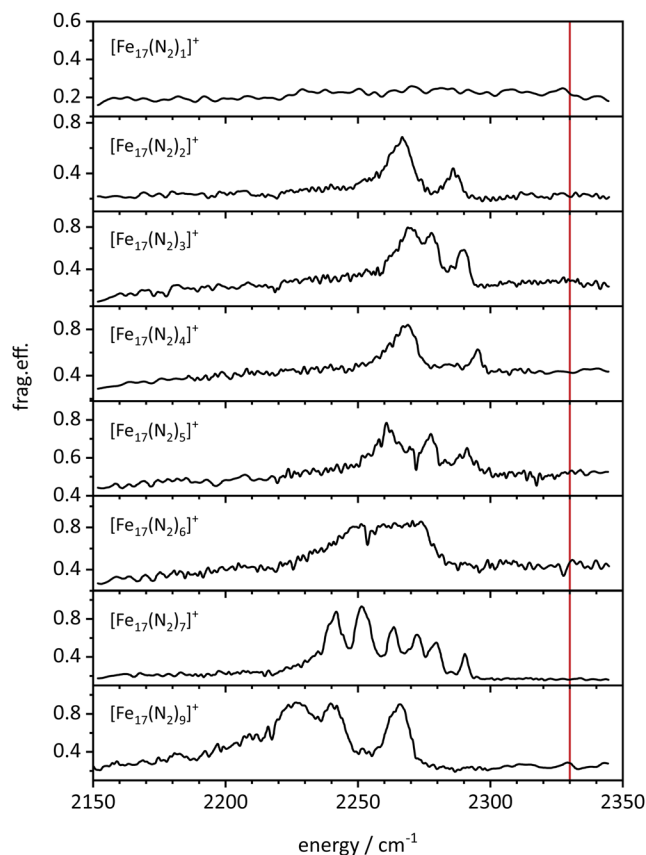


FIG. 9. IR-PD spectra of the (17, m) species at 26 K. The spectrum of (17,1) reveals no band but high non-resonant fragmentation, and the spectrum of (17,7) reveals well resolved structures, while all other spectra experience significant broadening. The vertical red line indicates the stretching frequency of the free N_2 moiety.

non-resonant fragmentation. We speculate that there must be some kind of weakly bound, almost roaming N_2 adsorbate, which is volatile and susceptible to swift desorption (cf. Fe_{17}^+ kinetics in CKS). This would imply a soft N_2 torsion, a broad distribution of N_2 orientations, and weak IR adsorption. The IR-PD spectra of “even” species (17,2) and (17,4) reveal two IR active bands at 2267 and 2286 cm^{-1} and at 2269 and 2295 cm^{-1} , respectively, indicating the likely presence of two binding motifs of N_2 . The “odd” species (17,3) and (17,5) reveal three bands at 2270, 2278, and 2290 cm^{-1} and at 2261, 2277, and 2291 cm^{-1} , respectively. Part of the (17,3) spectrum with the splitting of 8 cm^{-1} between the two most redshifted bands is reminiscent of symmetric/antisymmetric couplings of N_2 's at adjacent equivalent adsorption sites, as observed and analyzed in the cases of $[Ni_n(N_2)_m]^+$ investigated before.⁸⁰ The (17,5) spectrum is less well resolved and may allow for a similar interpretation but with high uncertainty. If so, the symmetric/asymmetric coupling of adjacent N_2 adsorbates would be significantly stronger as the coupling increased to about 20 cm^{-1} . The IR-PD spectrum of (17,6) is structureless with a single broad band (FWHM: 35 cm^{-1}) around 2265 cm^{-1} . This observation suggests that the adsorbate shell of six N_2 's on the surface of Fe_{17}^+ is highly fluxional and strongly coupled. One might speculate about a “molten” adsorbate layer, which would be most surprising in view of the prevailing cryo conditions. Alternatively, the couplings among the seven N_2 ligands might increase with respect to those of mere six N_2 ligands such that the bands would spread further and become more easily discernible.

Even more surprising is the observation of a completely different spectrum for (17,7), which is well structured. This cluster adsorbate complex reveals six sharp, separate bands at 2242, 2251, 2264, 2272, 2280, 2290 cm^{-1} . As before, the splitting of 8–10 cm^{-1} suggests the pairwise symmetric and antisymmetric coupling of N_2 adsorbates. It is remarkable to observe six resolved bands by seven N_2 chromophores, and it would take quantum chemical support to interpret this in detail (see below). In any case, we conclude that there can be little to no isomerism of (17,7) and suggest there must be a single distinct structure of the adsorbate layer. Thus, the (17,7) species is reminiscent of a “crystalline” adsorbate layer, which is in remarkable contrast to the suggested “molten” layer of (17,6).

The IR-PD spectrum of (17,9) reveals two broad and overlapping bands at 2227 and 2240 cm^{-1} and a narrower isolated band at 2266 cm^{-1} . This result indicates a degree of symmetry and structural definition that is lower than (17,7) but higher than (17,6). The spectrum comes close to that of (17,3), which suggests a symmetric/asymmetric splitting of 13 cm^{-1} for coupled N_2 oscillators, along with an interpretation of the 2266 cm^{-1} band as corresponding to an isolated N_2 adsorbate.

It would be most desirable to check all of the above interpretations and assignments against appropriate high-level quantum chemical calculations. There are some DFT predictions of naked Fe_{17} clusters published,^{66,68,69} which conclude that it has a capped hexagonal antiprism structure. Our own exploratory DFT studies at the PBE0 level find that the most stable structure has an icosahedral structural motif (cf. CKS, Fig. 14) with other structures conceivable. Unfortunately, it was impossible for us to conduct a systematic study of varying loads of N_2 adsorbates on these clusters. In this regard, as discussed below, the reduced level of theory (PBE) used to conduct

computational studies of a few (18, m) species did not provide useful spectroscopic information.

D. Fe_{18}^+

As noted above (Fig. 1), the (18, m) case reveals a far redshifted IR active region that is unique among all other investigated cluster sizes. Figure 10 shows spectra for $m = 1-16$. There are (multiple) bands in the region of 2120–2200 cm^{-1} in addition to the end-on IR active region of 2200–2310 cm^{-1} . There are at least three facts that may—in principle—contribute to spectral complexity and need to be considered when interpreting the observed spectra: (1) the Fe_{18}^+ structural isomerism as elucidated by kinetics (cf. CKS, Figs. 14 and S23), (2) the N_2 binding site isomerism, and (3) the N_2 coordination motif isomerism, where the binding motif might vary from on top (μ_1) via across edge (μ_2) to the above surface (μ_3). Our exploratory $Fe_{13}(N_2)_m^+$ DFT studies at the appropriate PBE0 level of

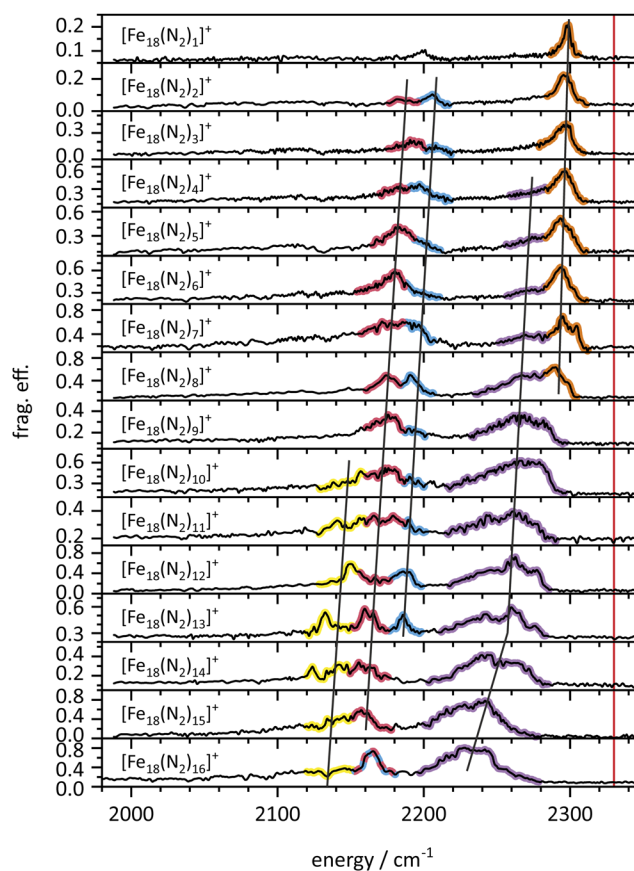


FIG. 10. Recorded IR-PD spectra of the (18, m) species at 26 K. All spectra reveal two IR active regions: from 2200 to 2320 cm^{-1} and from 2100 to 2200 cm^{-1} . Tentative assignments associate the orange and violet features with a $\mu_{1,end}$ N_2 coordination, where the violet motif represents the more tilted end-on binding motif $\mu_{1,tilt}$. The more redshifted blue, red, and yellow features may relate to various $\mu_{1,side}$ N_2 coordination motifs (further details; see the text). All binding motifs shift to red with increasing N_2 adsorption. The red vertical line indicates the stretching frequency of free N_2 .

theory (Fig. 4) revealed an unprecedented motif for (13,1)E, $\mu_{1,\text{side}}$, of an asymmetric bound side-on N_2 coordination $\mu_1\text{-}\kappa\text{N1,N2}$ with a stretching vibration at 2152 cm^{-1} , as well as a bridged μ_2 coordination motif (13,1)D, $\mu_2\text{-}\kappa\text{N1:}\kappa\text{N1,N2}$, with a stretching vibration at 1883 cm^{-1} . The novel $\mu_{1,\text{side}}$ motif of (13,1)E exhibits a N_2 stretching mode that coincides with the range of the more redshifted region ($2120\text{--}2200\text{ cm}^{-1}$) in the spectra of (18, m). We speculate that the novel $\mu_{1,\text{side}}$ motif might appear in (18, m) as well. In contrast, the bridging μ_2 coordination motif of (13,1) is significantly more redshifted and thus does not serve to explain the (18, m) observations. As a matter of fact, none of our spectra reveal IR intensity in the predicted range of bridging μ_2 coordination. Note that the novel $\mu_{1,\text{side}}$ motif becomes IR active by virtue of an asymmetric coordination with Fe–N distances that were predicted to differ by about 0.2 \AA in the case of (13,1) (cf. Fig. 4).

The observed variations of the presumed $\mu_{1,\text{side}}$ IR fingerprint in (18, m), marked as yellow, red, and blue IR features in Fig. 10, may originate from non-equivalent N-binding Fe sites. The Fe_{18}^+ cluster has a rougher cluster surface, as compared to smooth, symmetric Fe_{13}^+ . This could be a reason for a diversity of N_2 binding motifs and the accessibility of the presumed $\mu_{1,\text{side}}$ motif.

The IR bands of (18, m) in the region of $2200\text{--}2310\text{ cm}^{-1}$, marked as orange IR features, most likely correspond to the μ_1 end-on coordinated N_2 adsorbates, $\mu_{1,\text{end}}$. With higher N_2 coverage, mutual $\text{N}_2\text{--N}_2$ interactions might set in and increase gradually. In effect, the average N_2 tilt with respect to the surface normal might increase, leading to band broadening and shifts to the red for $m \geq 9$. These effects provide a tentative assignment of the observed violet IR features as a $\mu_{1,\text{tilt}}$ adsorption motif.

All marked binding motifs in Fig. 10 shift to the red with increasing N_2 adsorption. The blue $\mu_{1,\text{side}}$ and orange $\mu_{1,\text{end}}$ motif vanish at high N_2 coverages, with the orange motif lost earlier than the blue motif. The difference $\Delta\nu(\text{blue--orange}) \approx 100\text{ cm}^{-1}$ remains constant throughout the variation of N_2 load ($m = 2\text{--}8$). The yellow $\mu_{1,\text{side}}$ motif sets in late at $m \geq 10$. The major red $\mu_{1,\text{side}}$ and violet $\mu_{1,\text{end}}$ motifs observed at almost all N_2 coverages provide a constant difference of $\Delta\nu(\text{red--violet}) \approx 90\text{ cm}^{-1}$ up to $m = 13$. The redshift of $\approx 2\text{ cm}^{-1}$ per additional N_2 adsorbate for the violet features increases at $m \geq 14$ up to $\approx 4.5\text{ cm}^{-1}$ per additional N_2 adsorbate. The band at 2200 cm^{-1} of (18,1) splits when adsorbing further N_2 's. In the cases of (18,2), (18,3), (18,8), and (18,13), the red and blue regions exhibit distinct bands that are separated by $15\text{--}20\text{ cm}^{-1}$. This might indicate symmetric/antisymmetric N_2 stretching mode couplings with a slightly larger splitting than observed in the Ni– N_2 case.⁸⁰

Unfortunately, we cannot conduct a systematic DFT study of $\text{Fe}_{18}(\text{N}_2)_m^+$ complexes at the PBE0 because it would exceed our available computational resources. Our preliminary explorations at the reduced PBE level proved inappropriate and failed to predict any observed IR modes (Figs. S55/S59), as also observed in the cases of (13, m) and discussed above. Thus, the lack of explicit, high level DFT modeling precludes any definite assignments of the (18, m) IR-PD spectra. Nevertheless, the wealth of information from our kinetic studies, our IR experiments, and our exploratory DFT modeling of smaller clusters—most notably of (13,1)—allow for some valid speculation on the origin of the observed IR spectral features.

Despite our reluctance to utilize our DFT calculations at the PBE level for the interpretation of the IR-PD spectra, we, nevertheless, will examine the predicted structures, energetics, and spin couplings of some selected (18, m) species. We started our survey with three selected geometries of (18,0): icosahedral and hexagonal structural motifs, as documented in the literature,^{68–70,101} as well as a cubic-packed structure motif (Fig. S51). The computed stabilities of the icosahedral and the hexagonal structure are similar, whereas the cubic-packed motif is about 250 kJ/mol less stable (Fig. 11 and Fig. S51). In all three cases, we obtained clear preferences of high spin multiplicities: the icosahedral and hexagonal motifs get values of $2S + 1 = 56$ and 58 , respectively, and the less stable cubic packed motif gets $2S + 1 = 58$ as well. The addition of N_2 to any of the three Fe_{18}^+ structures, forming various $\text{Fe}_{18}(\text{N}_2)_m^+$ cluster adsorbate complexes, leads to a variety of different adsorbate geometries due to the variation of coordinating Fe centers as documented exhaustively in the supplementary material (Figs. S52–S59). Because our exploratory DFT calculations have reached their limits for these systems, we failed to obtain converged results in some cases. Nevertheless, it becomes discernible that stepwise N_2 adsorption induces stepwise spin quenching (Fig. 11)—a prediction that is well in line with the findings above for (13, m) clusters and recent findings in the case of Rhodium clusters: spin valleys shift lower upon higher adsorbate loads.¹⁰⁰

The kinetic studies of N_2 uptake by Fe_{18}^+ , cf. CKS, provide strong evidence for isomeric mixtures, tentatively assigned to a major component with a close packed structure (18cp) and a minor component with an icosahedral or hexagonal antiprismatic structure (18ico/18hex). The kinetics also suggest the conversion of a major isomer into a minor one upon uptake of some eight or nine N_2 adsorbate molecules. These kinetic findings correspond to the observation of the yellow feature and the disappearance of the orange ones in the IR spectra of (18, m) setting in around $m = 9$, the violet feature gradually setting in a little bit earlier.

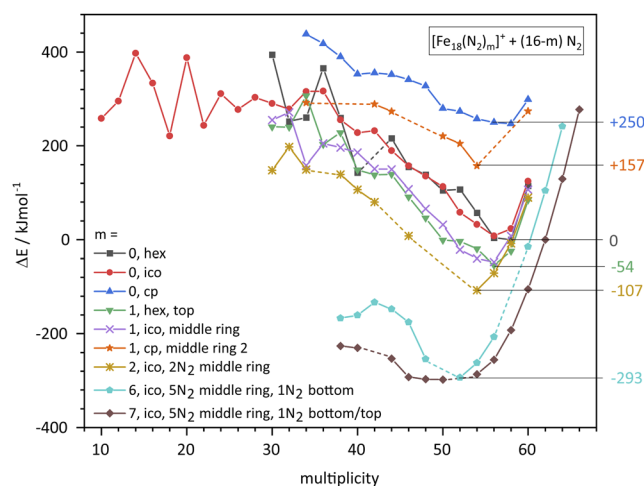


FIG. 11. Energetics of computed $[\text{Fe}_{18}(\text{N}_2)_m]^+$ cluster adsorbate structures (18, m) as a function of the spin multiplicity $2S + 1$, normalized to the most favorable (18,0) spin isomer (hexagonal, 58tet). The level of theory is PBE/def2TZVP.

IV. CONCLUSIONS

Our recorded IR-PD spectra of the cluster adsorbate complexes $[\text{Fe}_n(\text{N}_2)_1]^+$, abbreviated $(n,1)$, and $[\text{Fe}_n(\text{N}_2)_2]^+$, abbreviated $(n,2)$, for $n = 8-20$ revealed IR active bands in the region of $2150-2340 \text{ cm}^{-1}$. All investigated species, except $[\text{Fe}_{17}(\text{N}_2)_1]^+$, show at least one IR active band in the investigated region, and this band is most likely associated with stretching vibrations of end-on coordinated N_2 chromophores, the $\mu_{1,\text{end}}$ motif. These N_2 adsorbate bands are significantly redshifted with respect to the free N_2 stretching frequency (2330 cm^{-1}). In summary, the observed peak positions of first and second N_2 adsorbates, likely end-on, reveal little to no systematic variation. We take this finding as an indication for a largely equivalent bonding situation of the first and second N_2 adsorbate on the Fe_n^+ cluster surface. However, those complexes that exhibited special kinetic behavior are also special with respect to their IR spectra and vice versa.

The IR-PD spectra of $(13, m)$ reveal discernible couplings of proximate N_2 adsorbates setting in at $(13,3)$ and persisting up to $(13,5)$. On the basis of an icosahedral Fe_{13}^+ core structure, the observed $(13,6)$ sharp, single IR-PD band finds interpretation in terms of a high symmetry adsorbate arrangement, as also suggested by DFT modeling. The very fast kinetics of $(13,7-11)$ prevented any IR-PD spectra recordings for these clusters (cf. CKS). The first adsorbate shell closure at $(13,12)$ comes with extensive IR-PD band broadening resulting from more enhanced couplings, in line with the DFT modeling, which also predicts a spin quenching by N_2 adsorption as evidenced by the shift of the computed spin valleys (Fig. 8). Beyond these observations, the computed spectra provide the first hints of conceivable side-on and bridged coordination.

The IR-PD spectrum of $(17,1)$ surprisingly reveals an absence of any structure in the IR-PD spectrum but efficient non-resonant fragmentation. We speculate that there may be some kind of weakly bound, almost roaming, N_2 adsorbate, which is volatile and susceptible to swift desorption (cf. Fe_{17}^+ kinetics in CKS). The IR-PD spectra of $(17,m)$ show multiple and broad bands for all cases other than $(17,1)$ and $(17,7)$. We tentatively conclude that there is a high degree of variation in binding motifs and couplings of the N_2 adsorbates. In remarkable contrast, the six sharp and well separated bands in the IR-PD spectrum of $(17,7)$ suggest symmetric and antisymmetric couplings of pairwise equivalent N_2 adsorbates. An adsorbate load dependent reorganization among the N_2 adsorbates seems likely, and the concomitant structural volatility is consistent with the observed slow adsorption kinetics and high rates of desorption (cf. CKS).

The IR-PD spectra of $(18, m)$ reveal additional features in the $2120-2200 \text{ cm}^{-1}$ region, which we associate with a side-on $\mu_{1,\text{side}}$ ($\mu_1\text{-}\kappa\text{N}_1\text{,N}_2$) motif. We rule out a bridging μ_2 motif, which would come with a significantly larger redshift. The IR-PD bands of both the $\mu_{1,\text{end}}$ and $\mu_{1,\text{side}}$ motifs experience steady redshifts with increasing N_2 loadings. Interestingly, the $\mu_{1,\text{end}}$ associated IR-PD features are bimodal at medium N_2 loads, $(18,4)$ through $(18,8)$, and we conceive contributions of a $\mu_{1,\text{tilt}}$ adsorption motif at higher levels of N_2 loads. This phenomenon is possibly connected to structural relaxation of close-packed into icosahedral or antiprismatic hexagonal Fe_{18}^+ structures. Exploratory DFT modeling at the reduced PBE level proved inappropriate and failed to predict any observed IR modes, whereas more elaborate hybrid DFT modeling of the large cluster adsorbate complexes was computationally intractable.

Nevertheless, the exploratory PBE studies indicated some adsorbate-induced spin quenching as in the case of $(13,m)$ and as observed before in the case of $\text{Rh}_5^+(\text{N}_2)_m$.¹⁰⁰

SUPPLEMENTARY MATERIAL

See the [supplementary material](#) for spectra across extended frequency ranges, starting arrangements for DFT modeling, a comparison of computed cluster isomers with measured spectra, numerical values of spin isomers and spin contamination, and complementary levels of theory.

ACKNOWLEDGMENTS

This work was supported by the German Research Foundation DFG within the transregional collaborative research center SFB/TRR 88 “Cooperative effects in homo and heterometallic complexes” (3MET.de) and by the State Research Center OPTIMAS. P.B.A. acknowledges support from the National Science Foundation, Grant No. CHE-1954142. The ⁵⁶Fe pure isotope sample of this study was supplied by the United States Department of Energy Office of Science through the Isotope Program in the Office of Nuclear Physics. Quantum chemical modeling took place at the “Regionales Hochschulrechenzentrum Kaiserslautern” (RHRK). We thank Thomas Kolling for his technical assistance and valuable discussions. Finally, we would like to thank the reviewers for valuable comments.

AUTHOR DECLARATIONS

Conflict of Interest

A.S., M.P.K., D.V.F., S.D., J.M., and G.N.-S. conceived and conducted the experiments. A.S., C.W., and M.H.P. conducted the quantum chemical calculations. A.S., P.B.A., and G.N.-S. evaluated all data and wrote the manuscript, which all the authors revised and agreed to.

DATA AVAILABILITY

The data that support the findings of this study are available from the corresponding author upon reasonable request.

REFERENCES

- 1 T. Zambelli *et al.*, *Science* **273**, 1688 (1996).
- 2 J. K. Nørskov *et al.*, *J. Catal.* **209**, 275 (2002).
- 3 K. Honkala *et al.*, *Science* **307**, 555 (2005).
- 4 J. M. Thomas and W. J. Thomas, *Principles and Practice of Heterogeneous Catalysis* (John Wiley & Sons, 2014).
- 5 G. Ertl, H. Knözinger, and J. Weitkamp, *Handbook of Heterogeneous Catalysis* (CiteSeer, 1997), Vol. 2.
- 6 B. Cornils *et al.*, *Catalysis from A to Z: A Concise Encyclopedia* (John Wiley & Sons, 2020).
- 7 F. A. Khan, D. L. Steele, and P. B. Armentrout, *J. Chem. Phys.* **99**, 7819 (1995).
- 8 B. L. Tjelta and P. B. Armentrout, *J. Phys. Chem. A* **101**, 2064 (1997).
- 9 B. L. Tjelta, D. Walter, and P. B. Armentrout, *Int. J. Mass Spectrom.* **204**, 7 (2001).
- 10 C. Berg, G. Nieder-Schatteburg, and V. E. Bondybey, *Second International Conference on Low Temperature Chemistry* (BkMk Press, Kansas City, MO, 1996), Vol. 1.
- 11 R. Schlögl and S. B. Abd Hamid, *Angew. Chem., Int. Ed.* **43**, 1628 (2004).

- ¹²A. Nilsson, L. G. Pettersson, and J. Norskov, *Chemical Bonding at Surfaces and Interfaces* (Elsevier, 2011).
- ¹³S. M. Lang and T. M. Bernhardt, *Phys. Chem. Chem. Phys.* **14**, 9255 (2012).
- ¹⁴P. B. Armentrout, *Catal. Sci. Technol.* **4**, 2741 (2014).
- ¹⁵E. L. Muetterties and J. Stein, *Chem. Rev.* **79**, 479 (1979).
- ¹⁶G. Ertl, *Angew. Chem., Int. Ed. Engl.* **47**, 3524 (2008).
- ¹⁷M. D. Morse *et al.*, *J. Chem. Phys.* **83**, 2293 (1985).
- ¹⁸A. Mittasch and W. Frankenburg, in *Advances in Catalysis*, edited by W. G. Frankenburg, V. I. Komarewsky, and E. K. Rideal (Academic Press, 1950), p. 81.
- ¹⁹R. Schlögl, *Ammonia Synthesis in Handbook of Heterogeneous Catalysis* (Wiley-VCH Verlag GmbH & Co. KG, 2008), Vol. 2.
- ²⁰J. R. Jennings, *Catalytic Ammonia Synthesis: Fundamentals and Practice* (Springer Science & Business Media, 2013).
- ²¹H. Liu, *Ammonia Synthesis Catalysts: Innovation and Practice* (World Scientific, 2013).
- ²²F. Bozso *et al.*, *J. Catal.* **49**, 18 (1977).
- ²³F. Bozso, G. Ertl, and M. Weiss, *J. Catal.* **50**, 519 (1977).
- ²⁴G. Ertl, S. B. Lee, and M. Weiss, *Surf. Sci.* **114**, 515 (1982).
- ²⁵M. Grunze *et al.*, *Phys. Rev. Lett.* **53**, 850 (1984).
- ²⁶H.-J. Freund *et al.*, *Surf. Sci.* **185**, 187 (1987).
- ²⁷M. C. Tsai *et al.*, *Surf. Sci.* **155**, 387 (1985).
- ²⁸C. N. R. Rao and G. R. Rao, *Surf. Sci. Rep.* **13**, 223 (1991).
- ²⁹J. J. Mortensen *et al.*, *J. Catal.* **182**, 479 (1999).
- ³⁰J. J. Mortensen *et al.*, *Surf. Sci.* **422**, 8 (1999).
- ³¹L. J. Whitman *et al.*, *Phys. Rev. Lett.* **56**, 1984 (1986).
- ³²M. A. Duncan, *Annu. Rev. Phys. Chem.* **48**, 69 (1997).
- ³³M. A. Duncan, *Int. Rev. Phys. Chem.* **22**, 407 (2003).
- ³⁴N. R. Walker, R. S. Walters, and M. A. Duncan, *New J. Chem.* **29**, 1495 (2005).
- ³⁵J. Roithová, *Chem. Soc. Rev.* **41**, 547 (2012).
- ³⁶J. Oomens *et al.*, *Int. J. Mass Spectrom.* **254**, 1 (2006).
- ³⁷L. MacAleese and P. Maitre, *Mass Spectrom. Rev.* **26**, 583 (2007).
- ³⁸W. Schöllkopf *et al.*, in *Advances in X-Ray Free-Electron Lasers Instrumentation III* (International Society for Optics and Photonics, 2015), p. 95121L.
- ³⁹M. Okumura, L. I. Yeh, and Y. T. Lee, in *Laser Spectroscopy VII*, edited by T. W. Hänsch and Y. R. Shen (Springer, Berlin, Heidelberg, 1985), p. 122.
- ⁴⁰M. Okumura, L. I. Yeh, and Y. T. Lee, *J. Chem. Phys.* **88**, 79 (1988).
- ⁴¹L. Jiang *et al.*, *J. Am. Chem. Soc.* **132**, 7398 (2010).
- ⁴²M. Z. Kamrath *et al.*, *J. Am. Chem. Soc.* **133**, 6440 (2011).
- ⁴³A. B. Wolk *et al.*, *Acc. Chem. Res.* **47**, 202 (2014).
- ⁴⁴S. Dillinger *et al.*, *Phys. Chem. Chem. Phys.* **17**, 10358 (2015).
- ⁴⁵I. Swart *et al.*, *J. Phys. Chem. A* **112**, 1139 (2008).
- ⁴⁶D. M. Kiawi *et al.*, *J. Phys. Chem. Lett.* **7**, 2381 (2016).
- ⁴⁷A. Fielicke *et al.*, *Surf. Sci.* **603**, 1427 (2009).
- ⁴⁸J. T. Lyon *et al.*, *J. Chem. Phys.* **131**, 184706 (2009).
- ⁴⁹C. P. McNary and P. B. Armentrout, *Phys. Chem. Chem. Phys.* **16**, 26467 (2014).
- ⁵⁰G. Blyholder, *J. Chem. Phys.* **68**, 2772 (1964).
- ⁵¹J. Dewar, *Bull. Soc. Chim. Fr.* **18**, C71 (1951).
- ⁵²J. Chatt and L. A. Duncanson, *J. Chem. Soc.* **1953** 2939.
- ⁵³G. L. Gutsev, M. D. Mochena, and C. W. Bauschlicher, Jr., *J. Phys. Chem. A* **108**, 11409 (2004).
- ⁵⁴A. Jedidi *et al.*, *Theor. Chem. Acc.* **133**, 1430 (2014).
- ⁵⁵A. Fielicke *et al.*, *J. Am. Chem. Soc.* **125**, 11184 (2003).
- ⁵⁶A. Fielicke *et al.*, *J. Chem. Phys.* **124**, 194305 (2006).
- ⁵⁷E. D. Pillai, T. D. Jaeger, and M. A. Duncan, *J. Phys. Chem. A* **109**, 3521 (2005).
- ⁵⁸E. D. Pillai, T. D. Jaeger, and M. A. Duncan, *J. Am. Chem. Soc.* **129**, 2297 (2007).
- ⁵⁹A. D. Brathwaite, H. L. Abbott-Lyon, and M. A. Duncan, *J. Phys. Chem. A* **120**, 7659 (2016).
- ⁶⁰C. Kerpel *et al.*, *J. Phys. Chem. C* **117**, 12153 (2013).
- ⁶¹S. Shetty, A. P. J. Jansen, and R. A. van Santen, *J. Phys. Chem. C* **112**, 17768 (2008).
- ⁶²M. Castro and D. R. Salahub, *Phys. Rev. B* **49**, 11842 (1994).
- ⁶³P. Ballone and R. O. Jones, *Chem. Phys. Lett.* **233**, 632 (1995).
- ⁶⁴T. Oda, A. Pasquarello, and R. Car, *Phys. Rev. Lett.* **80**, 3622 (1998).
- ⁶⁵D. Hobbs, G. Kresse, and J. Hafner, *Phys. Rev. B* **62**, 11556 (2000).
- ⁶⁶O. Diéguez *et al.*, *Phys. Rev. B* **63**, 205407 (2001).
- ⁶⁷G. Rollmann, P. Entel, and S. Sahoo, *Comput. Mater. Sci.* **35**, 275 (2006).
- ⁶⁸G. L. Gutsev *et al.*, *J. Phys. Chem. A* **116**, 10218 (2012).
- ⁶⁹H. K. Yuan *et al.*, *J. Chem. Phys.* **139**, 034314 (2013).
- ⁷⁰A. Jedidi *et al.*, *Phys. Chem. Chem. Phys.* **16**, 20703 (2014).
- ⁷¹H. A. Duarte *et al.*, *Inorg. Chem.* **38**, 3895 (1999).
- ⁷²T. L. Haslett *et al.*, *J. Am. Chem. Soc.* **122**, 6039 (2000).
- ⁷³B. Chen *et al.*, *Phys. Chem. Chem. Phys.* **23**, 2166 (2021).
- ⁷⁴S. K. Loh *et al.*, *J. Chem. Phys.* **90**, 5466 (1989).
- ⁷⁵L. Lian, C. X. Su, and P. B. Armentrout, *J. Chem. Phys.* **97**, 4072 (1992).
- ⁷⁶J. Conceição *et al.*, *J. Chem. Phys.* **104**, 3976 (1996).
- ⁷⁷J. B. Griffin and P. B. Armentrout, *J. Chem. Phys.* **106**, 4448 (1997).
- ⁷⁸L. Tan, F. Liu, and P. B. Armentrout, *J. Chem. Phys.* **124**, 084302 (2006).
- ⁷⁹R. Liyanage, J. B. Griffin, and P. B. Armentrout, *J. Chem. Phys.* **119**, 8979 (2003).
- ⁸⁰S. Dillinger, J. Mohrbach, and G. Niedner-Schatteburg, *J. Chem. Phys.* **147**, 184305 (2017).
- ⁸¹J. Mohrbach, S. Dillinger, and G. Niedner-Schatteburg, *J. Phys. Chem. C* **121**, 10907 (2017).
- ⁸²J. Mohrbach, S. Dillinger, and G. Niedner-Schatteburg, *J. Chem. Phys.* **147**, 184304 (2017).
- ⁸³M. P. Klein *et al.*, *Top. Catal.* **61**, 106 (2018).
- ⁸⁴S. Dillinger *et al.*, *J. Phys. Chem. Lett.* **9**, 914 (2018).
- ⁸⁵D. V. Fries *et al.*, *Phys. Chem. Chem. Phys.* **23**, 11345 (2021).
- ⁸⁶A. Straßner *et al.* “Kinetics of stepwise nitrogen adsorption by size-selected iron cluster cations: Evidence for size-dependent nitrogen phobia,” (to be published).
- ⁸⁷M. Frisch *et al.*, *Gaussian 09* (Gaussian, Inc., Wallingford, CT, 2009).
- ⁸⁸M. J. Frisch *et al.*, *Gaussian 16* (Gaussian Inc., Wallingford, CT, 2016).
- ⁸⁹J. P. Perdew, K. Burke, and M. Ernzerhof, *Phys. Rev. Lett.* **77**, 3865 (1996).
- ⁹⁰C. Adamo and V. Barone, *J. Chem. Phys.* **110**, 6158 (1999).
- ⁹¹J. Tao *et al.*, *Phys. Rev. Lett.* **91**, 146401 (2003).
- ⁹²V. N. Staroverov *et al.*, *J. Chem. Phys.* **119**, 12129 (2003).
- ⁹³F. Weigend and R. Ahlrichs, *Phys. Chem. Chem. Phys.* **7**, 3297 (2005).
- ⁹⁴W. M. Haynes, *CRC Handbook of Chemistry and Physics* (CRC Press/Taylor & Francis, Boca Raton, Florida, 2012), Vol. 93.
- ⁹⁵C. N. R. Rao, G. R. Rao, and K. Ppabhakaran, *Chem. Phys. Lett.* **134**, 47 (1987).
- ⁹⁶M. Niemeyer *et al.*, *Phys. Rev. Lett.* **108**, 057201 (2012).
- ⁹⁷M. Wu *et al.*, *Phys. Rev. B* **86**, 174410 (2012).
- ⁹⁸J. Meyer *et al.*, *J. Chem. Phys.* **143**, 104302 (2015).
- ⁹⁹A. Salzer, *Pure Appl. Chem.* **71**, 1557 (1999).
- ¹⁰⁰A. A. Ehrhard *et al.*, *Mol. Phys.* **119**, e1953172 (2021).
- ¹⁰¹Q.-M. Ma *et al.*, *Solid State Commun.* **142**, 114 (2007).
- ¹⁰²“tet” refers to the multiplicity as common for small spin values in singlet, doublet, etc. A 4tet thus refers to $2S + 1 = 46$, which implies 45 unpaired electrons with parallel spins.